Methane C-H Activation by $[Cu_2O]^{2+}$ and $[Cu_3O_3]^{2+}$ in Copper-Exchanged Zeolites: Computational Analysis of Redox Chemistry and X-ray Absorption Spectroscopy

Olabisi Suleiman[#], Dipak Panthi[#], Olajumoke Adeyiga[#] and Samuel O. Odoh*

Department of Chemistry, University of Nevada Reno, 1664 N. Virginia Street, Reno, NV 89557-0216

Email Addresses:

osuleiman@unr.edu

dpanthi@unr.edu

oadeyiga@unr.edu

sodoh@unr.edu

Abstract: There is an ongoing debate regarding the role of $[Cu_3O_3]^{2+}$ in methane-to-methanol conversion (MMC) by copper-exchanged zeolites. Here, we use electronic structure analysis and localized orbital bonding analysis, LOBA, to probe the redox chemistry of its Cu and μ-oxo sites. Also, the X-ray absorption near-edge structure, XANES, of methane activation in $[Cu_3O_3]^{2+}$ is compared to the more ubiquitous $[Cu_2O]^{2+}$. Methane C-H activation is associated with only the Cu^{2+}/Cu^{+} redox couple in $[Cu_2O]^{2+}$. For $[Cu_3O_3]^{2+}$, there is no basis for the Cu^{3+}/Cu^{2+} couple's participation, at the density functional theory (DFT) ground state. In $[Cu_3O_3]^{2+}$, there are many possible intra-zeolite intermediates for methane activation. In the 9 possibilities that we examined, methane activation is driven by a combination of the Cu^{2+}/Cu^{+} and oxyl/O^{2-} redox couples. Based on this, the Cu 1s-edge XANES spectra of $[Cu_2O]^{2+}$ and $[Cu_3O_3]^{2+}$ should both have energy signatures of $Cu^{2+} \rightarrow Cu^{+}$ reduction during methane activation. This is indeed what we obtained from the calculated XANES spectra. $[Cu_2O]^{2+}$ and $[Cu_3O_3]^{2+}$ intermediates with 1 Cu^{+} site are shifted by 0.9-1.7 eV while those with 2 Cu^{+} sites are shifted by 3.0-4.2 eV. These are near the range of 2.5-3.2 eV observed experimentally after contacting methane with activated copper-exchanged zeolites. Thus, activation of methane by $[Cu_3O_3]^{2+}$ will lead to formation of Cu^{+} sites. Importantly for future quantitative XANES studies, involvement of $O^{-} + e^{-} \rightarrow O^{2-}$ in $[Cu_3O_3]^{2+}$ implies a disconnect between the overall reactivity and the number of electrons used in the Cu^{2+}/Cu^{+} redox couple.

Keywords: Copper-exchanged zeolites, active sites, methane activation, X-ray absorption spectra, redox chemistry, time-dependent density functional theory, oxidation states.

1. INTRODUCTION

Natural gas reserves are abundant across the globe. Natural gas consists mostly of methane, which is a valuable source of energy and industrial chemicals.[1,2] As such, conversion of methane to liquid derivatives like methanol is the target of many research efforts. Efficient and direct conversion of methane to methanol will likely be more cost-effective than current liquefaction techniques.[3,4] Of the various systems that are active towards the methane C-H bond, copper-exchanged zeolites have garnered great interest.[5-13] The active sites for converting methane to methanol in these zeolites are known to be small copper oxo species. There however is some debate about the exact nature of these species.[14-16] Several mono-copper, dicopper and tri-copper species have been proposed.[17,18] However, invocation of a unique tri-copper tri-oxo, $[Cu_3O_3]^{2+}$,[19-25] active site species complicates established description of the Cu^{2+}/Cu^{+} redox couple as the driver for conversion of methane to methanol.[26] Quantum-mechanical calculations revealed the presence of mixed-valence Cu^{2+}/Cu^{3+} oxidation states for the Cu centers in $[Cu_3O_3]^{2+}$.[14] Additionally, two of the μ-oxo sites in $[Cu_3O_3]^{2+}$ possess oxyl character, which were suggested as being suitable for methane C-H activation.[14] This implies that methane-to-methanol conversion, MMC, is associated with no change in the oxidation states of the Cu centers. However, Cu^{2+}/Cu^{3+} components of its wavefunction would suggest that MMC is driven by the Cu^{3+}/Cu^{2+} redox couple in $[Cu_3O_3]^{2+}$, at least in part. Thus, analysis of its electronic structure during methane C-H activation is required. This will allow for detailed understanding of how methane C-H activation affects the $[Cu^{2+}, 2Cu^{3+}, 3O^{2-}]^{2+}$ or $[3Cu^{2+}, 2O^{-}, O^{2-}]^{2+}$ configurations of $[Cu_3O_3]^{2+}$.[12]

Until recently, there was little computational evidence for the spectroscopic properties of zeolites containing $[Cu_3O_3]^{2+}$. Initially, Grundner et al.[22] fitted the EXAFS spectrum of $[Cu_3O_3]^{2+}$ in zeolite mordenite, MOR, to the calculated spectrum of a structure obtained from density functional theory, DFT.[12,27,28] However, we more recently showed that the broad absorption bands at 31000 and 38000 cm^{-1} in the UV-Vis spectra are linked to $[Cu_3O_3]^{2+}$.[29] For this, we employed a long-range corrected double hybrid density functional for Tamm-Dancoff time-dependent DFT, TDA-DFT, calculations.[30] This functional is ωB2PLYP.[31-33] ωB2PLYP also captures the decrease in the intensities of the 30000 and 38000 cm^{-1} bands upon contact with methane.[34] This agrees very well with the experimental data.[22,35,36] These reports on computational evidence for the spectroscopic properties of $[Cu_3O_3]^{2+}$ are encouraging. However, there has been no detailed analysis of how methane C-H activation affects the formal oxidation states of the Cu and μ-oxo sites in $[Cu_3O_3]^{2+}$.

Additionally, there are currently no reports in the literature for quantum-mechanical computations of the Cu 1s-edge X-ray absorption near-edge structure, XANES, spectra for $[Cu_3O_3]^{2+}$. Interestingly, XANES spectra of $[Cu_3O_3]^{2+}$ can reveal how the oxidation states of its Cu sites are altered after methane hydroxylation. Indeed, it remains to be seen whether changes induced by methane activation in the XANES spectra of $[Cu_3O_3]^{2+}$ are similar to those for other copper-oxo active sites.

2. METHODOLOGY

2.1. Systems of Interest: A cluster model for the mono-(μ-oxo) dicopper, $[Cu_2O]^{2+}$ active site in zeolite ZSM-5[37] is shown in Figure 1. This active site has been extensively characterized in various zeolites.[6,10,12,38-41] As such, we can use it as a reference for comparing the $[Cu_3O_3]^{2+}$ system. The cluster model, **1A**, has been used by us previously.[29,34] This 47-atom model includes the complete first- and second-coordination spheres around the dicopper active site. After activating methane, there are several possible intermediate species that can be formed. These are also shown in Figure 1. At low methane pressures, the methyl group can rebound to another $[Cu_2O]^{2+}$ site, **1B**, while the abstracted proton is bound to the reacting $[Cu_2O]^{2+}$, **1C**. However, at high methane pressures, the separated methyl could rebound back to the reacting $[Cu_2O]^{2+}$ site,

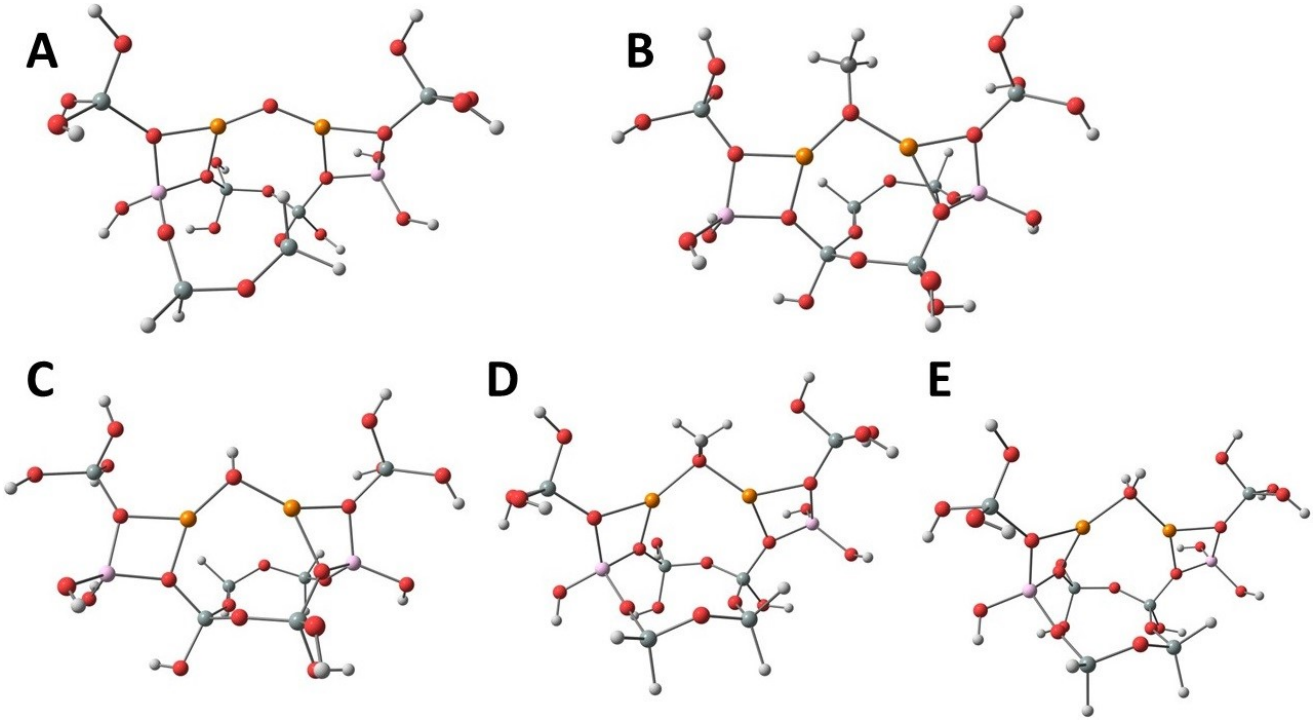

Figure 1: Optimized structures of the cluster models of $[Cu_2O]^{2+}$. **A** is the cluster model for the active site. **B**-**E** are intermediates formed after methane C-H activation.

forming a [Cu-O(H)(CH_3)-Cu] moiety, **1D**. Structures **1B-1D** have been previously proposed. We also need to consider the situation where the methyl group is stabilized at a basic framework oxo atom. In this situation, only **1C** is of interest. If the separated methyl group stabilizes at a Brønsted acid site, in exchange for the acidic proton, then **1C** and **1E** are of interest. In Table 1, we provide a summary of the properties of **1A-1E**.

Table 1: Summary of $[Cu_2O]^{2+}$ species of interest.

	1A	**1B**	**1C**	**1D**	**1E**
Copper-oxo cluster	Yes				
C-H activation intermediate		Yes	Yes	Yes	Yes
High/Low Methane pressures	Both	Likely low	Likely low	Possibly high	Possibly both

A cluster model for the $[Cu_3O_3]^{2+}$ site in the eight-membered ring, 8MR, of MOR is shown in Figure 2. This model has been used previously by various workers.[14,29,34] In addition to $[Cu_3O_3]^{2+}$, **2A**, we considered several possible intermediates formed after C-H activation. In some of these, the methyl group and H from methane are coordinated to two μ-oxo atoms at the active site. These are labeled as **2B**, **2C** and **2D** in Figure 2. However, the methyl group could rebound back to the reactive μ-oxo atom, leading to **2E**. If the methyl is stabilized at a Brønsted acid site, in exchange for the acidic proton, then **2F** and **2G** are of interest. At high pressures, 2 methane molecules can

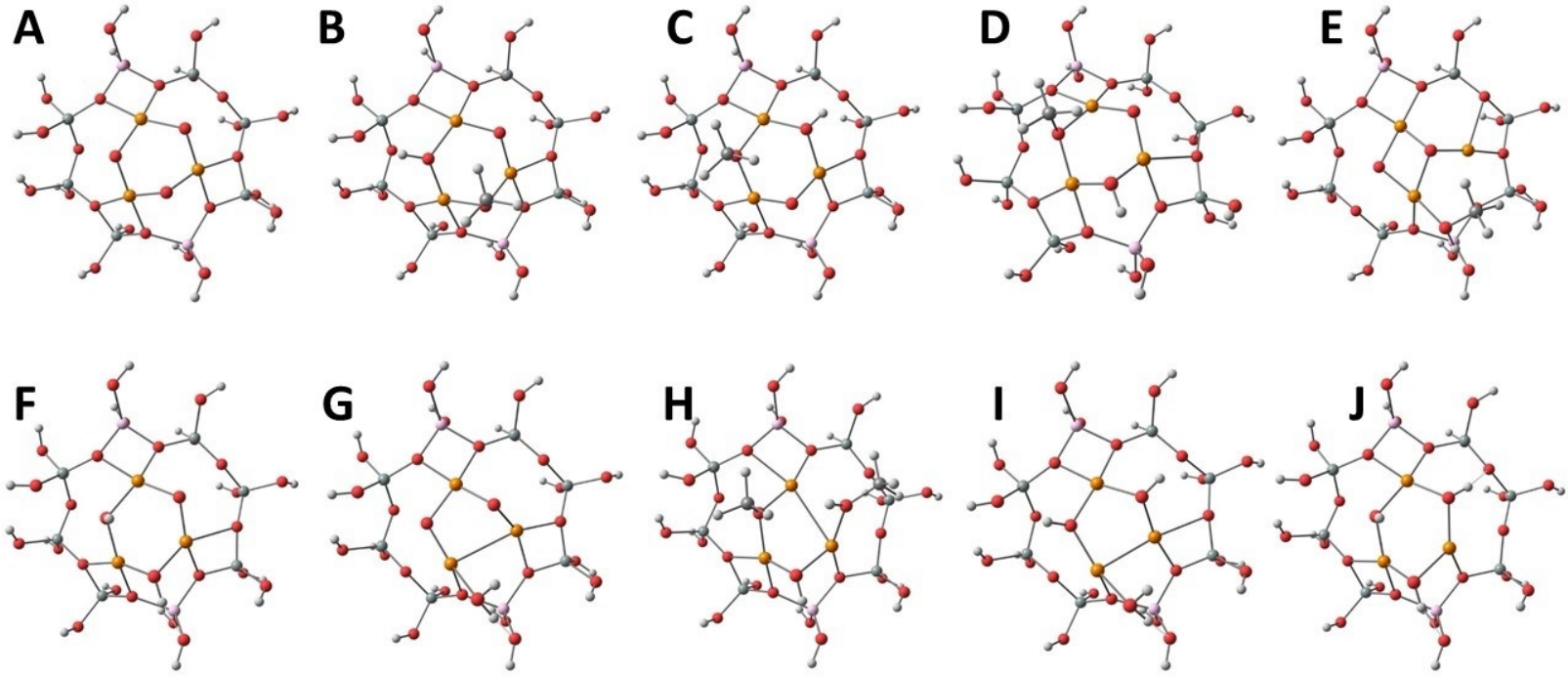

Figure 2: Optimized structures of the cluster models of $[Cu_3O_3]^{2+}$. **A** is the cluster model for the active site. **B-J** are possible intrazeolite intermediates formed after methane C-H activation.

can be activated by $[Cu_3O_3]^{2+}$, leading to the structures shown as **2F** and **2H**. In **2H**, both methyl groups rebound to the extra-framework copper-oxo site. This structure is very similar to that examined previously by Zheng et al.[42] In **2F**, both methyl groups are stabilized away from the active site. Lastly, if both methyl groups are remotely stabilized via exchange with Brønsted acid sites, then **2I** and **2J** are of interest. The possible intra-zeolite intermediates for $[Cu_3O_3]^{2+}$ are definitely more numerous than for $[Cu_2O]^{2+}$. In Table 2, we provide a summary of the properties of **2A**-**1J**.

Table 2: Summary of $[Cu_3O_3]^{2+}$ species of interest.

	Copper-oxo cluster	C-H activation intermediate	High/Low Methane pressures
2A	Yes		Both
2B		Yes	Likely low
2C		Yes	Likely low
2D		Yes	Likely low
2E		Yes	Likely low
2F		Yes	Possibly both
2G		Yes	Possibly both
2H		Yes	High
2I		Yes	High
2J		Yes	High

2.2 Geometry Optimizations: The cluster models were all optimized with the B3LYP-D3BJ [43-46] functional while using def2-SVP[47] basis sets. Vibrational frequency analyses were performed in order to confirm the local minimal of these structures. We neglected 1-2 low frequency imaginary modes, less than 150 cm^{-1}, associated with the terminating protons.

2.3 Localized Orbital Bonding Analysis: Single-point calculations were performed on the optimized geometries at the ωB2LYP/cc-pVDZ, B3LYP/cc-pVDZ, ωB2LYP/cc-pVTZ and B3LYP/cc-pVTZ levels.[48,49] B3LYP is often used to study transition metal complexes[50], while ωB2LYP provides a good description of the ground state electronic structures of copper oxo species.[29,34] Localized Orbital Bonding Analyses, LOBA, were carried out on the converged self-consistent-field solutions in order to determine the formal oxidation states of the atoms in our cluster models.[51] The threshold for performing LOBA was set to 46-50%. This was sufficient to ensure that the sum of the oxidation states of all atoms was 0. All calculations were performed with the unrestricted DFT formalism.

2.4 TDA-DFT Calculations of Near-Edge X-ray Absorption Spectra: X-ray absorption spectra for the Cu K-edge were also calculated with TDA-DFT. In all cases, the Cu 1s core orbitals

were localized and only excitations from these into virtual orbitals were allowed. We requested 200-450 excited states in our calculations. Quadrupole corrections to the oscillator strengths were also calculated. Scalar-relativistic effects were accounted for with the Zeroth Order Regular Approximation, ZORA.[52] We used minimally-augmented ma-ZORA-def2-TZVPP basis sets.[53,54] For XANES TDA-DFT calculations, we used the B1LYP functional with 20% Hartree-Fock exchange and 80% DFT exchange.[49,55,56] This functional, B1LYP-20%, provides the least relative deviations for the pre-edge features of two Cu complexes. The benchmark dataset used for this comparison were from the report by Wieghardt et al.[57], Supporting Information (SI). Calculated XANES spectra were fitted with Gaussian functions with FWHM of 1.3 eV (10485 cm^{-1}).

2.5. Software: All DFT and TDA-DFT calculations were performed with the Orca software code, version 4.2.1.[58,59] We used the Multiwfn software for LOBA.[60]

3. RESULTS AND DISCUSSIONS

3.1. Localized Orbital Bonding Analysis and Electronic Structure Analysis

We first discuss the oxidation states and electronic structure properties of the $[Cu_2O]^{2+}$ and $[Cu_3O_3]^{2+}$clusters. We compare their properties to those of intrazeolite intermediates formed after methane activation.

3.1.1 Mono(μ-oxo) dicopper active site: The calculated oxidation states for the Cu and μ-oxo atoms of $[Cu_2O]^{2+}$ in **1A** are shown in Figure 3. Oxidation states after methane activation to form **1B**-**1E** are also shown. Before methane activation, the $[Cu_2O]^{2+}$ site has a $[2Cu^{2+}, \mu\text{-}O^{2-}]$ character. LOBA shows that methane activation is facilitated by reduction of 2 Cu^{2+} sites to Cu^{+}, Figure 3. There is a Cu^{+} site in **1B** and another in **1C**. In essence, **1B** and **1C** both have $[Cu^{+}, \mu\text{-}O^{2-}, Cu^{2+}]$ characters. **1D** and **1E** both have 2 Cu^{+} sites and are thus of $[Cu^{+}, \mu\text{-}O^{2-}, Cu^{+}]$ character. In all cases, the oxidation state of the μ-oxo atom remains unchanged at -2, Figure 2.

The results from LOBA can be explained by examining the canonical orbitals for the singlet state of $[Cu_2O]^{2+}$. $[Cu_2O]^{2+}$ has a restricted singlet state ground state. However as we used unrestricted DFT, we are left with singly-occupied MOs. Before methane activation, there are four occupied frontier molecular orbitals, MOs, that are heavily dominated (60-75%) by contributions from the μ-oxo atom, Figure 4. These contain four electrons (2α and 2β). There are also significant μ- oxo 2p contributions to several other MOs, ranging from 6-30%. One of these is shown in Figure 4. It is thus reasonable that the oxidation state of the μ-oxo atom is -2, corresponding to a full octet. Both Cu atoms have only minor contributions, < 3%, to these high-lying valence orbitals. In **1B**

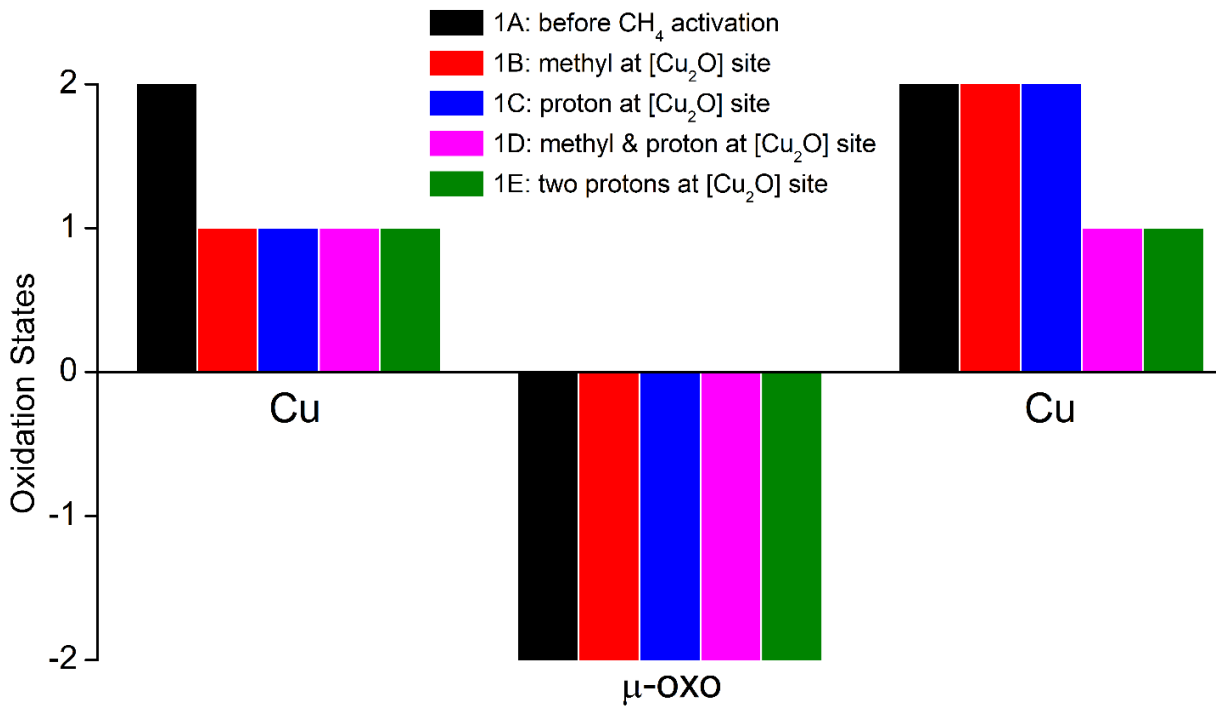

Figure 3: Formal oxidation states from LOBA for Cu and μ-oxo atoms of $[Cu_2O]^{2+}$ in various structures. cc-pVDZ and cc-pVTZ basis sets were used with B3LYP and ωB2LYP.

and **1C**, the nature of the frontier orbitals change dramatically, Figure 5. The μ-oxo 2p orbitals are stabilized, due to hybridization with orbitals of the separated methyl group and proton from methane, Figure 5. To allow this, an electron is shifted out of a μ-oxo 2p orbital in **1B** and **1C** into Cu 3d orbitals, which now dominate the highest occupied MOs, Figure 5. A similar mechanism is responsible for reduction of 2 Cu^{2+} sites in **1D** and **1E**.

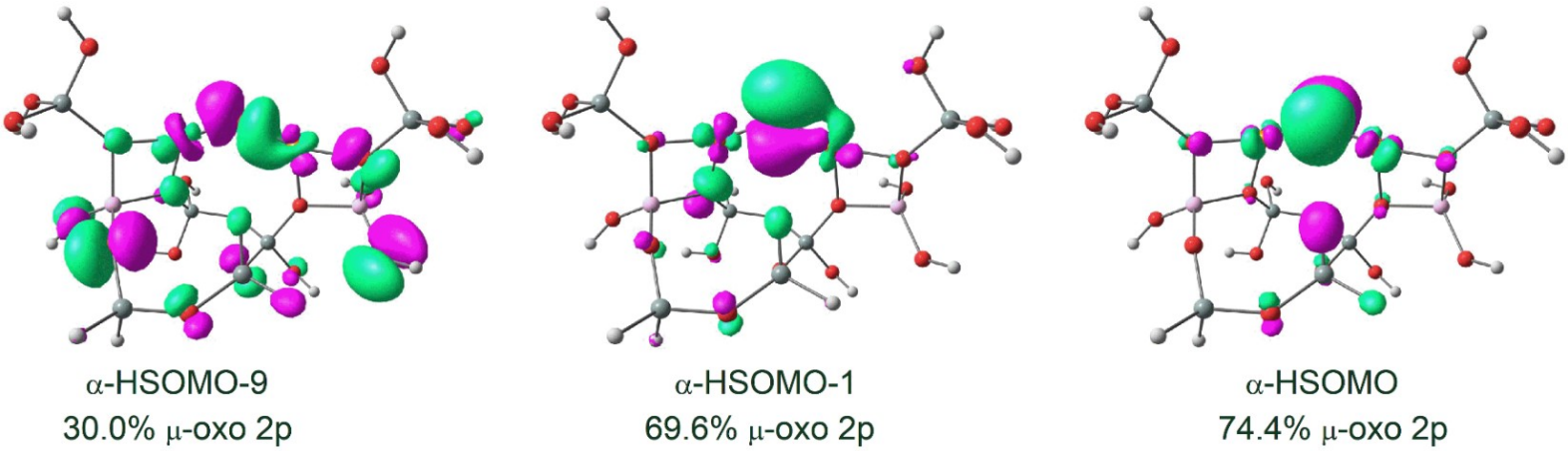

Figure 4: Frontier orbitals of the α-electron manifold in $[Cu_2O]^{2+}$, **1A**, at ωB2LYP/cc-pVTZ level.

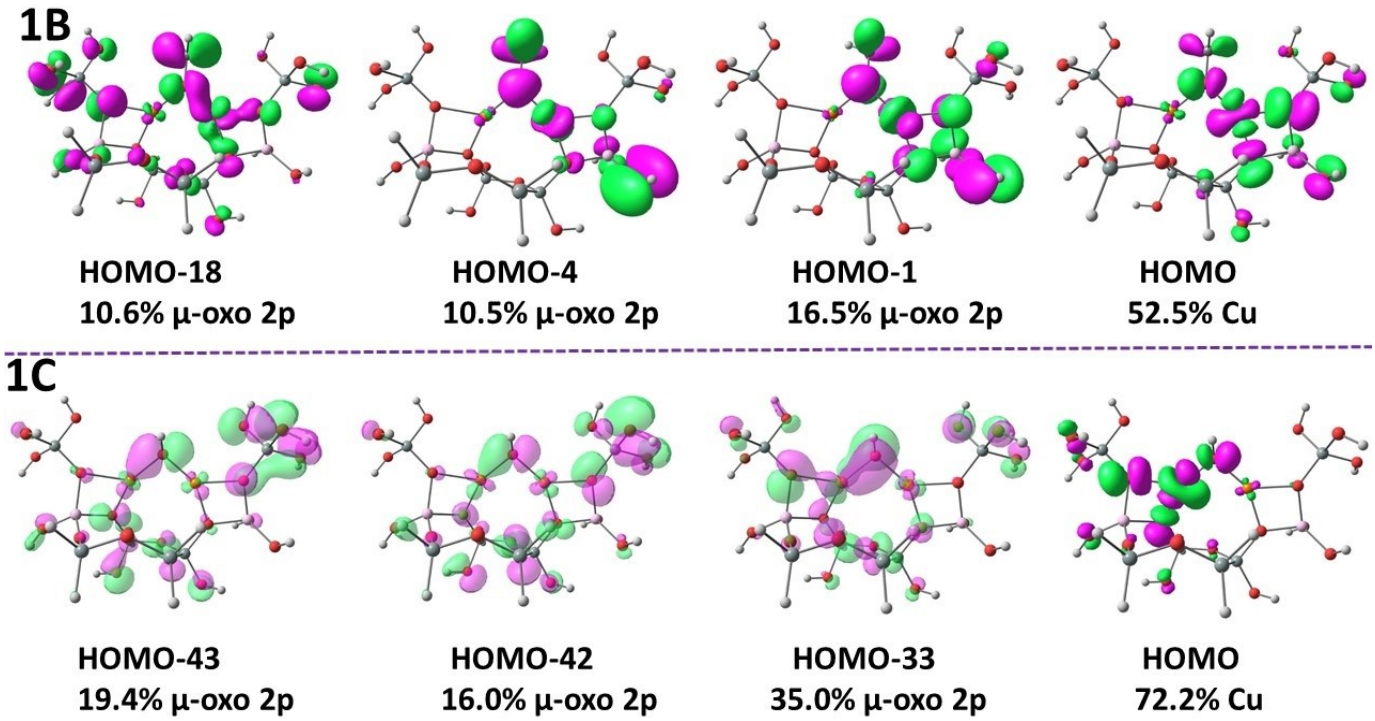

Figure 5: Frontier α-orbitals in $[Cu_2O]^{2+}$ after methane hydroxylation. Some orbitals of the μ-oxo atom with CH_3 and H from methane are shown with transparent lobes for better visualization.

3.1.2 Tris(μ-oxo) tricopper active site: We now discuss the results from LOBA and electronic structure analysis for $[Cu_3O_3]^{2+}$ and the possible intra-zeolite intermediates formed after its reaction with methane, Figure 2. Before methane C-H activation, **2A**, the three Cu centers in $[Cu_3O_3]^{2+}$ are all Cu^{2+}, Figure 6. This concurs with Löwdin spin densities of 0.84, -0.79 and 0.85 on these sites, at the ωB2LYP/cc- pVTZ level. The oxidation states of the three μ-oxo atoms are -1, -1 and -2, in agreement with the previously described anisotropy of $[Cu_3O_3]^{2+}$.[12] Thus, **2A** has a configuration of $[3Cu^{2+}, 2O^{-}, O^{2-}]^{2+}$, with 2 oxyl sites available for interaction with methane.

For the intermediate species, we first consider the species in which the separated methyl group(s) is(are) stabilized at μ-oxo atom(s) of the active site. These are **2B**-**2D** as well as **2H**. We first differentiate between **2B** and **2C** on the one hand and **2D** on the other. For **2B** and **2C**, LOBA with B3LYP and ωB2LYP reveal that the oxidation states of the Cu centers remain unchanged, Figure 6. For these 2 structures, methane C-H activation is *seemingly* accompanied by reduction of both oxyl sites, $2O^{-} + 2e^{-} \rightarrow 2O^{2-}$. This transfer of electrons can be seen by examining the canonical MOs, Figure 7. Prior to methane activation, the frontier orbital, HSOMO to HSOMO-3 are delocalized over the μ-oxo oxyl and O^{2-} sites. After C-H activation in **2B**, the occupied frontier orbitals are localized on an erstwhile oxyl, converting it into O^{2-}. Indeed, LOBA indicates

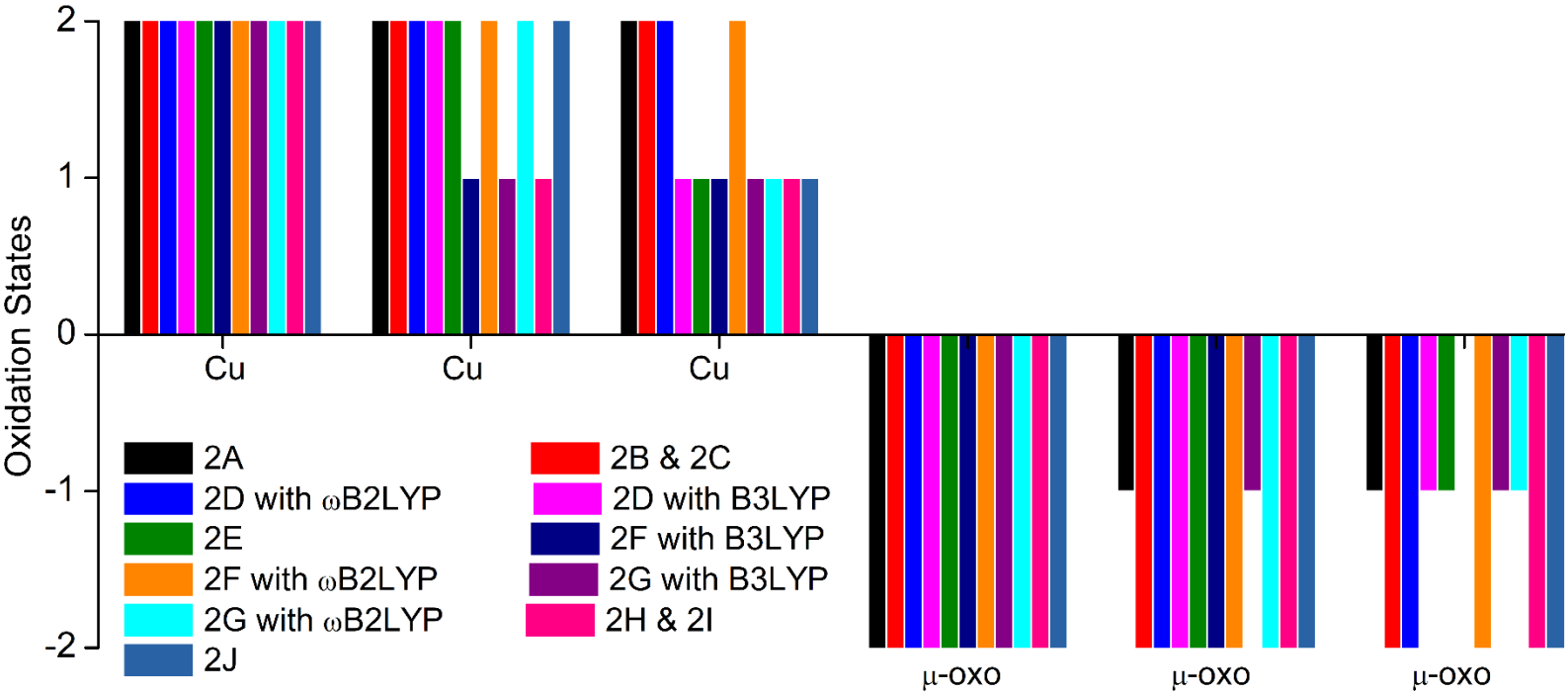

Figure 6: Formal oxidation states from LOBA for Cu and μ-oxo atoms of $[Cu_3O_3]^{2+}$ before and after methane hydroxylation. These were performed on converged solutions with cc-pVTZ basis sets. For structures **2D**, **2F** and **2G**, we present LOBA results from ωB2LYP and B3LYP.

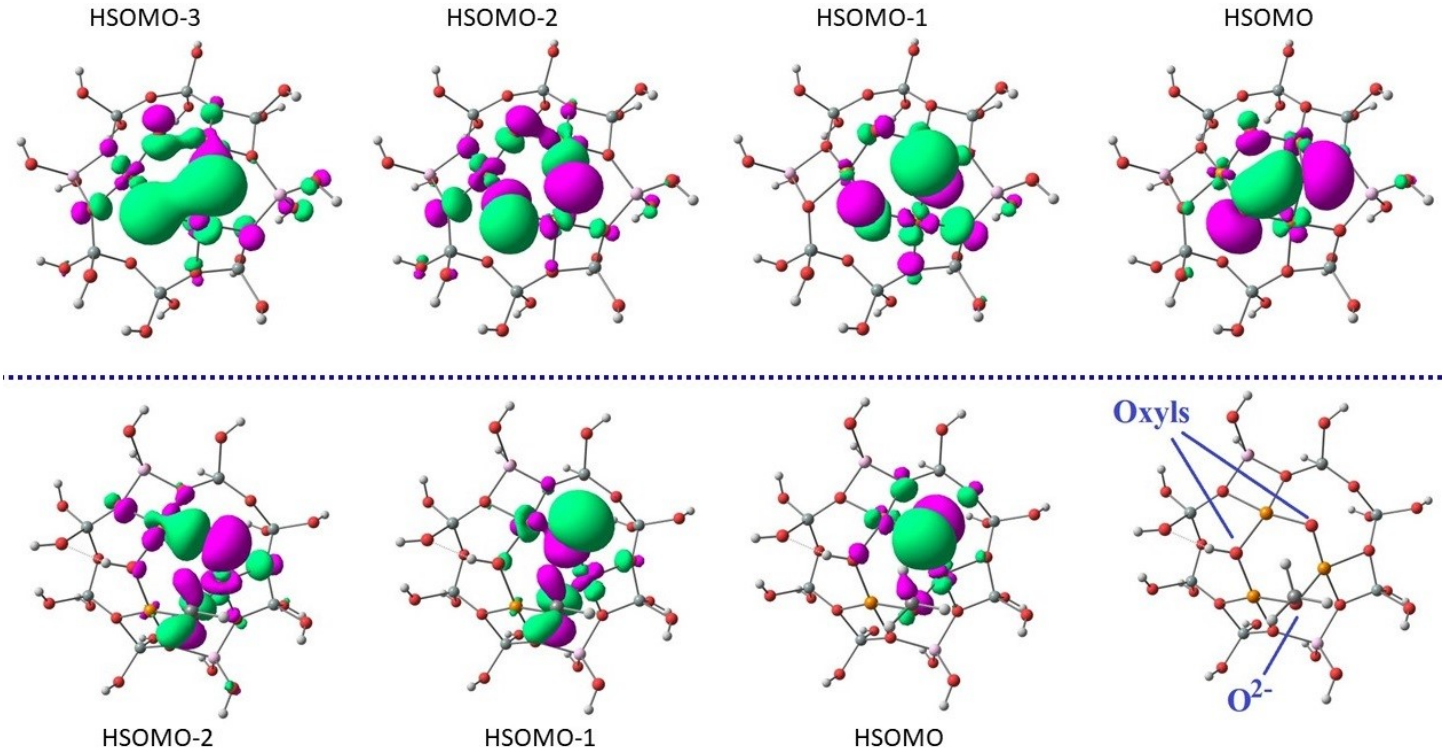

Figure 7: Frontier orbitals of the α-electron manifold in $[Cu_3O_3]^{2+}$, **2A**, (*top*) and after (*bottom*) methane C-H activation in structure **2B**.

that the CH_3 group has an oxidation state of +1, suggesting electron transfer of the sort: $CH_3^{\cdot} + O^{2-} + O^{-} \rightarrow CH_3^{+} + 2O^{2-}$. Hybridization with H 1s converts the other oxyl site to O^{2-}. In **2C**, both oxyl sites are hybridized with H 1s and C 2p orbitals, converting them both to O^{2-}. This corresponds to $CH_3^{\cdot} + H^{\cdot} + 2O^{-} \rightarrow CH_3^{+} + H^{+} + 2O^{2-}$.

For **2D**, we obtained different results from LOBA on the ωB2LYP and B3LYP solutions, Figure 6. For ωB2LYP with cc-pVTZ and cc-pVDZ basis sets, both oxyl sites are reduced to O^{2-}, just as in **2B** and **2C**. However, with B3LYP, only one oxyl site is reduced to O^{2-}. The other electron is transferred to a Cu^{2+} site, reducing it to Cu^{+}. This result from B3LYP suggests that methane activation to yield **2D** is associated with partial contributions from the Cu^{2+}/Cu^{+} and oxyl/O^{2-} redox couples. B3LYP is a global hybrid with 20% Hartree-Fock (HF) exchange while ωB2LYP is a truncated range-separated hybrid functional with 53% and 100% HF exchange in the short- and long-range, respectively. Thus, ωB2LYP likely favors excessive localization of electrons.

We can provide some clear statements about our findings, Figure 6. First, these ground state DFT and LOBA results provide no support for involvement of the Cu^{3+}/Cu^{2+} redox couple in methane activation by $[Cu_3O_3]^{2+}$. Second, the Cu^{2+}/Cu^{+} redox couple definitely plays a role in methane activation by $[Cu_3O_3]^{2+}$. Indeed, we are quite confident that LOBA's assignment of three Cu^{2+} and three O^{2-} sites for **2D** with ωB2LYP is due to a borderline partitioning threshold. To explain this, let us revisit **2B** and **2C**, briefly. The μ-oxo 2p-dominated frontier orbitals of the new O^{2-} (erstwhile oxyl not bound to H or CH_3), Figure 7, actually contain 12.7-28.6% contributions from Cu. This is at the ωB2LYP/cc-pVTZ level, demonstrating clearly that **2B** and **2C** also have appreciable Cu^{+} characters. Turning back to **2D**, with B3LYP, the contributions from Cu to HSOMO, HSOMO-1 and HSOMO-2 are 38.3%, 35.0% and 42.6%, respectively. As such, LOBA assigned an electron to a Cu site and one oxyl site remains, Figure 6. However with ωB2LYP, contributions from Cu to these orbitals are slightly lower, 42.5%, 34.6% and 37.9%, respectively. This functional also slightly reduces delocalization to framework aluminate oxos. As such, LOBA assigned both electrons to the erstwhile oxyl site, resulting in an oxidation state of -2, Figure 6. These analyses reinforce our conclusion that methane activation by $[Cu_3O_3]^{2+}$ is driven by a combination of the Cu^{2+}/Cu^{+} and oxyl/O^{2-} redox couples. Thus, spectroscopic characterizations of this active site *must* indicate signatures of intrazeolite $Cu^{2+} \rightarrow Cu^{+}$ reduction during MMC. This must be especially true for **2D**, and indeed for **2B** and **2C**, albeit likely to lesser extents.

Overall, our analysis for these intermediates indicate that there would be 1 mole of Cu^+ produced for each mole of activated methane.

All other $[Cu_3O_3]^{2+}$ intermediates involve the Cu^{2+}/Cu^+ redox couple, to some extent, Figure 6. **2E** involves $Cu^{2+} + e^- \rightarrow Cu^+$ and $O^- + e^- \rightarrow O^{2-}$ with B3LYP and ωB2LYP. Interestingly, **2F** involves $2Cu^{2+} + 2e^- \rightarrow 2Cu^+$ and $O^- + e^- \rightarrow O^{2-}$ as well as $O^- \rightarrow O + e^-$ at the B3LYP/cc-pVTZ level. At the ωB2LYP/cc-pVTZ level, the only redox process is $2O^- + 2e^- \rightarrow 2O^{2-}$. Similarly, **2G** involves only $2Cu^{2+} + 2e^- \rightarrow 2Cu^+$ with B3LYP but $Cu^{2+} + e^- \rightarrow Cu^+$ and $O^- + e^- \rightarrow O^{2-}$ with ωB2LYP. The differences are related to the amount of HF exchange in the functionals.

For species considered to be relevant at high methane pressures, **2H** and **2I** involve $2Cu^{2+} + 2e^- \rightarrow 2Cu^+$ and $2O^- + 2e^- \rightarrow 2O^{2-}$ while **2J** involves $Cu^{2+} + e^- \rightarrow Cu^+$ and $2O^- + 2e^- \rightarrow 2O^{2-}$. In these cases, B3LYP and ωB2LYP agree with each other. For **2H** and **2I**, 4 electrons are released from 2 methane molecules, whereas for **2J**, a methyl group departs with 1 of the released electrons. The formal oxidation states of all μ-oxo atoms in **2H** and **2I** are -2. Both oxyl sites and two Cu^{2+} sites are reduced, Figure 6. As noted earlier, the Löwdin spin densities of the Cu atoms in **2A** are 0.84, -0.79 and 0.85 at the ωB2LYP/cc- pVTZ level. After activation of 2 methane molecules, these are 0.00, 0.01 and 0.83 in **2H**. This is clear evidence for $3Cu^{2+} + 2e^- \rightarrow 2Cu^+ + Cu^{2+}$. Similarly, the spin densities on the μ-oxo atoms were -0.53, -0.41 and 0.97 in **2A**. In **2H**, they are 0.05, 0.08 and 0.00, evidence for $2O^- + O^{2-} + 2e^- \rightarrow 3O^{2-}$. We see similar trends for **2I**.

3.2. TDA-DFT XANES Spectra for $[Cu_2O]^{2+}$ Models

In this section, we consider the Cu 1s edge spectra of the $[Cu_2O]^{2+}$ sites as well as the intermediate species shown in Figure 1. This is interesting as XANES spectra have been extensively used to quantify the amount of Cu^+ produced after contacting copper-exchanged zeolites with methane. At the Cu 1s-edge, a rising edge peak near 8986 eV is assigned to 1s → 4p electronic transitions in Cu^{2+} centers. These are shifted to about 8983 eV after $Cu^{2+} \rightarrow Cu^+$ reduction. This 2.5-3.2 eV shift after Cu^{2+} one-electron reduction has been reported by various workers.[22,61-63] One would thus expect that the calculated near-edge X-ray absorption spectra of our $[Cu_2O]^{2+}$ cluster models would also show some shift. This would be a way to confirm the involvement of the Cu^{2+}/Cu^+ redox couple in methane activation by $[Cu_2O]^{2+}$ and $[Cu_3O_3]^{2+}$, Figures 3 and 6.

The calculated spectra for the $[Cu_2O]^{2+}$ species are shown in Figure 8. The first dominant electronic transition is calculated to be at 8992.7 eV in **1A**. After methane activation, the earliest dominant transitions are at 8991.2 and 8991.1 eV in **1B** and **1C**, respectively. The XANES spectra are shifted

by 1.5 and 1.6 eV, respectively. These are below shifts of 2.5-3.2 eV observed empirically.[22,61-63] The absolute transition energies from TDA-DFT are somewhat inaccurate. However, we are mainly interested in comparing the XAS shifts with $[Cu_3O_3]^{2+}$ systems.

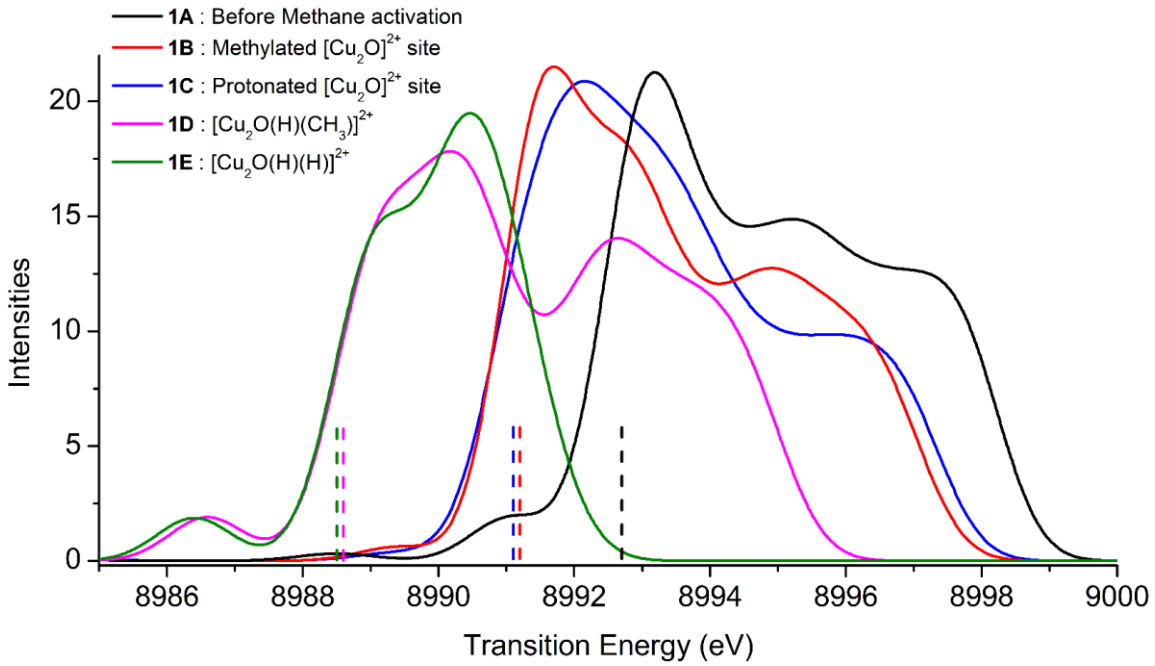

Figure 8: Calculated Cu 1s-edge spectra of $[Cu_2O]^{2+}$ species, **1A-1E**. Pre-edge 1s → 3d and near-edge 1s → 4s/4p peaks are of interest in characterizing the Cu oxidation states.

For, **1D** and **1E**, the 1s → 4p transitions are shifted by 4.1-4.2 eV, Figure 8. These are greater than the 2.5-3.2 eV shifts often observed experimentally. **1D-1E** both have 2 Cu^+ sites while **1B-1C** only have a Cu^+ site, Figure 3. It thus appears that the XAS shifts predicted by TDA-DFT are related to the number of Cu^+ sites in our cluster models.

3.3. TDA-DFT XANES Spectra for $[Cu_3O_3]^{2+}$ Models

For the $[Cu_3O_3]^{2+}$ system, the most intense Cu 1s → 4s/4p transition is at 8992.3 eV in **2A**, Figures 9 and 10. Thus, prior to methane C-H activation, the Cu 1s → 4p transition energies are essentially the same in $[Cu_3O_3]^{2+}$ and $[Cu_2O]^{2+}$. This makes sense, given that the Cu centers in these species are all Cu^{2+}, Figures 3 and 6. For the intermediates, the first dominant Cu 1s → 4p transitions are shifted to 8990.9, 8991.4, 8990.6, 8990.2, 8990.7, 8989.3, 8988.0, 8988.1 and 8988.0 eV for **2B**, **2C**, **2D**, **2E**, **2F**, **2G**, **2H**, **2I** and **2J**, respectively, Figures 9 and 10. Relative to **2A**, the XAS spectra of **2B**, **2C**, **2D**, **2E**, **2F**, **2G**, **2H**, **2I** and **2J** are shifted by 1.4, 0.9, 1.7, 2.1, 1.6, 3.0, 4.3, 4.2 and 4.3 eV, respectively. The shifts for **2B-2D** and **2F** are less than shifts of 2.5-3.2 eV shifts observed experimentally. [22,61-63] By contrast, the calculated shifts for **2H-2I** are significantly larger than 2.5-

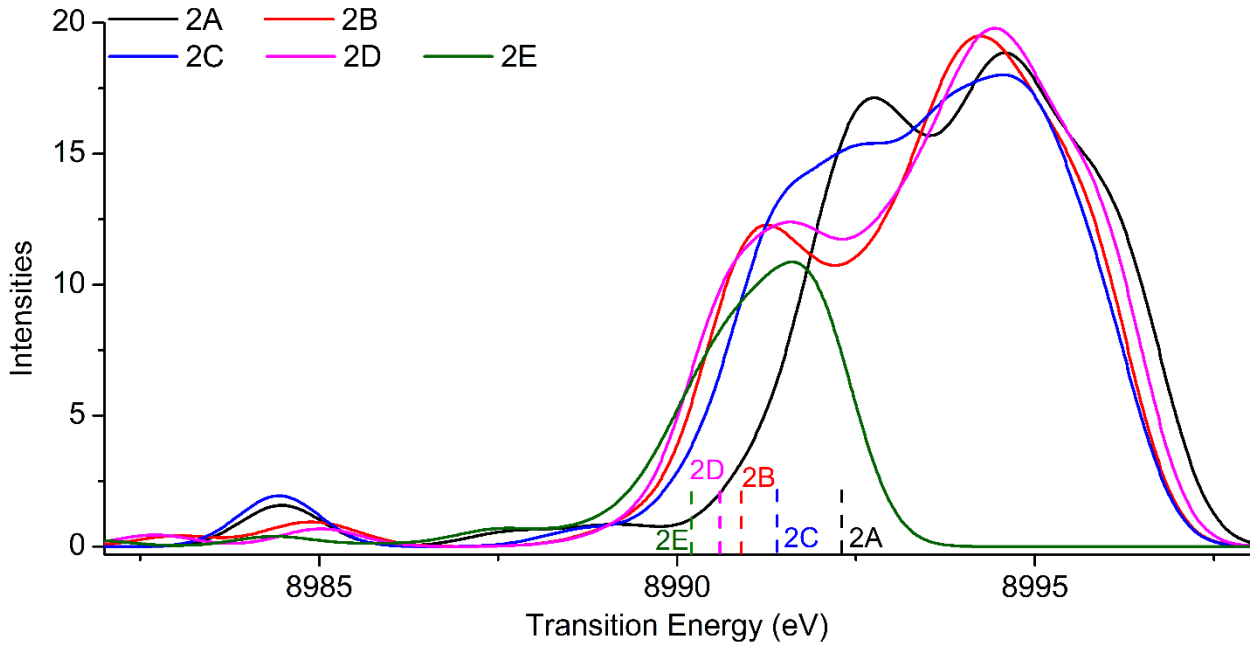

Figure 9: Cu 1s-edge spectra of $[Cu_3O_3]^{2+}$ species, **2A**-**2E**. The earliest dominant pre-edge Cu 1s → 4s/4p peaks are indicated with dashed lines.

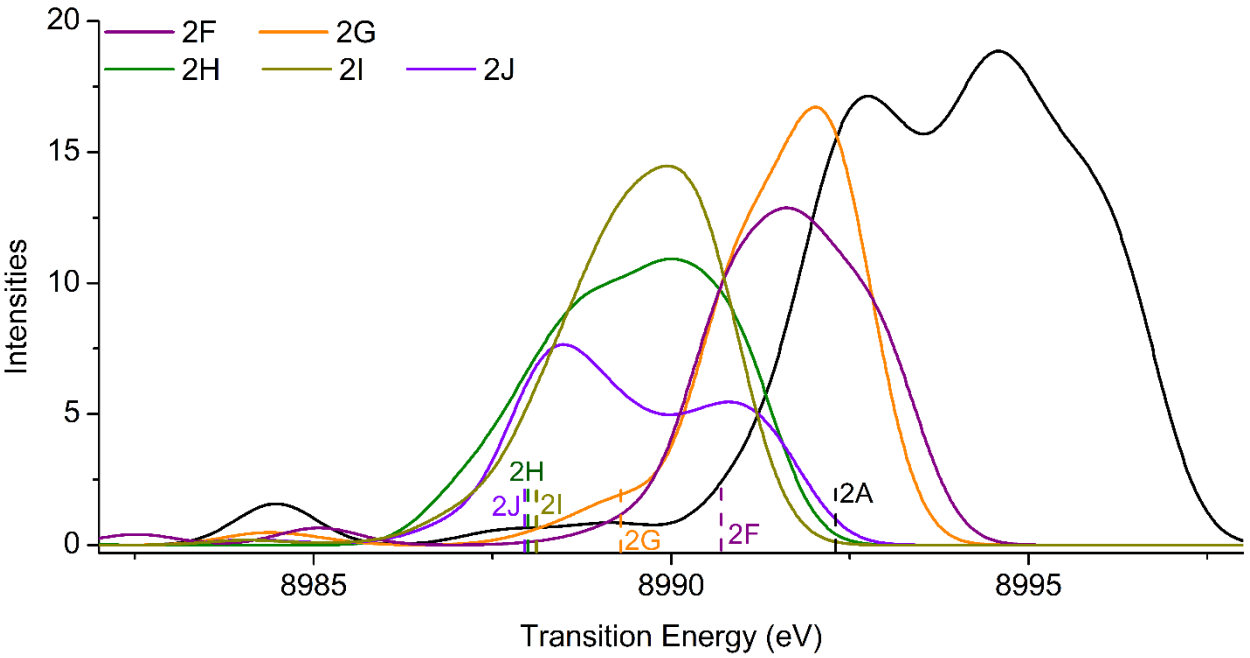

Figure 10: Calculated Cu 1s-edge spectra of $[Cu_3O_3]^{2+}$ species, **2A** as well as **2F**-**2J**. The earliest dominant pre-edge Cu 1s → 4s/4p peaks are indicated with dashed lines.

3.2 eV while that of **2G** falls within the range of empirical data. This is similar to the situation for $[Cu_2O]^{2+}$ species. Species with only 1 Cu^+ site, Figure 6, yield XAS shifts smaller than 2.5-3.2 eV while species with 2 Cu^+ sites predict XAS shifts significantly larger than 2.5-3.2 eV. Indeed, the

shifts obtained for **2B-2F** match well to those obtained for **1B-1C**, while those for **2H-2I** match well with results for **1D-1E**. This confirms the presence of one or more Cu^+ sites in the $[Cu_3O_3]^{2+}$ species. Moreover, for the $[Cu_3O_3]^{2+}$ species, the lowest-energy dominant Cu 1s → 4s/4p transitions are from the 1s orbitals localized precisely on the Cu atoms involved in $Cu^{2+} \rightarrow Cu^+$ reduction. We conclude that $[Cu_2O]^{2+}$ and $[Cu_3O_3]^{2+}$ sites would show identical signature energy shifts due to Cu^+ in XANES spectra. This is quite likely to be the case at low- or high-methane pressures. Our results in Figures 6 and 9 strongly indicate that, *assuming 100% selectivity*, 1 mole of Cu^+ will always be produced per mole of methane activated by $[Cu_3O_3]^{2+}$.

3.4. Impact of Cluster Model Size and Structural Dynamics

We have also checked the dependence of our results on the size of our cluster models as well as the structural dynamics under finite temperature conditions. We first enlarged our models by adding more framework atoms, Figure 11. For these larger clusters, we considered species analogous to **1A**, **1C**, **2A**, **2F** and **2I**. Details for the computational protocols for these larger clusters are given in the Supporting Information. In all cases, results from LOBA for the larger models species are the same as for their smaller counterparts. Thus, our smaller models are sufficient for describing the electronic structures of the copper-oxo sites. As noted earlier, the smaller models already capture the first- and second-coordination spheres of the active sites.

We also carried out ab initio molecular dynamics (AIMD) simulations on the periodic structures of species corresponding to **2A**, **2F** and **2I**. For each, 3 simulations were carried out for 8 ps, using initial structures from an initial 8 ps equilibration step. Our AIMD protocol is similar to that used previously by Li et al.[64] We randomly selected 20 structures from the post-equilibrium trajectory files. Cluster models similar to those in Figure 2 were constructed from the selected structures. The positions of the Cu, O, Al and Si atoms were kept fixed while the positions of terminating hydrogen atoms were optimized.

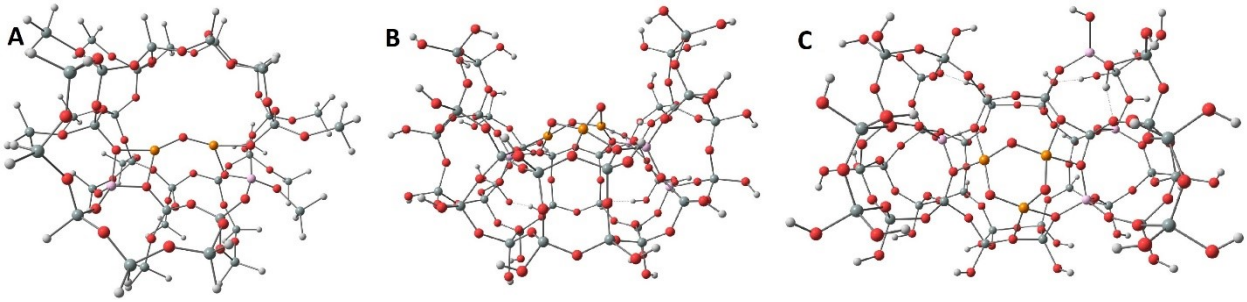

Figure 11: Larger cluster models of the $[Cu_2O]^{2+}$ and $[Cu_3O_3]^{2+}$ species. The dicopper complex is shown in **(A)** while 2 views of the tricopper species are given in **(B)** and **(C)**.

LOBA results for all AIMD structures for **2A** and **2I** were unchanged from results presented in Figure 6. For **2F**, structures from AIMD involve $Cu^{2+} + e^- \rightarrow Cu^+$ and $O^- + e^- \rightarrow O^{2-}$ at the B3LYP/cc-pVTZ level. This is compared with $2Cu^{2+} + 2e^- \rightarrow 2Cu^+$; $O^- + e^- \rightarrow O^{2-}$ and $O^- \rightarrow O + e^-$ for the DFT-optimized structure. Crucially, all AIMD and DFT geometries involve the Cu^{2+}/Cu^+ reduction. Calculated XAS shifts for AIMD geometries are shown in Table 3. Overall, spectra for **2F** and **2I** are respectively shifted by 0.9-2.4 and 2.9-4.2 eV relative to **2A** structures. These ranges cover the shifts of 1.6 and 4.2 eV obtained with DFT-optimized structures, Figure 10. Thus, structural dynamics are important for accurate reproduction of the Cu 1s-edge spectra of the copper-oxo species. However, regarding the crux of the current work, the calculated XAS shifts indicative of $Cu^{2+} \rightarrow Cu^+$ reduction still exist after using structures sampled from AIMD trajectories. These XAS shifts will be evident in $[Cu_2O]^{2+}$ and $[Cu_3O_3]^{2+}$ species.

Table 3: Calculated shifts (eV) in Cu 1s-edge spectra of several $[Cu_3O_3]^{2+}$ species.

	2A	**2F**	**2I**
DFT geometry	8992.3	8990.7	8988.1
Calculated Shift	0.0	1.6	4.2
AIMD geometries	8992.0-8992.8	8990.4-8991.1	8988.6-8989.1
Calculated Shift	0.0	0.9-2.4	2.9-4.2

CONCLUSIONS

We have investigated the redox behavior of Cu and oxo atoms in 2 active sites capable of converting methane to methanol in copper-exchanged zeolites. Specifically, we compared the $[Cu_3O_3]^{2+}$ and $[Cu_2O]^{2+}$ active sites. We analyzed the electronic structures of these systems with Density Functional Theory (DFT) and Localized Bond Orbital Analysis, LOBA. We used Tamm-Dancoff Approximation DFT, TDA-DFT, to compute the Cu 1s-edge X-ray absorption spectra (XAS) of these species. We also considered intra-zeolite intermediates formed after methane C-H activation at low- and high- methane pressures, for both copper-oxo sites.

Prior to methane activation, the ground state of $[Cu_3O_3]^{2+}$ has a configuration of $[3Cu^{2+}, 2O^-, O^{2-}]^{2+}$, at the DFT level. This configuration indicates three Cu^{2+} sites, 2 oxyl sites and an O^{2-} site. By a similar token, $[Cu_2O]^{2+}$ has a $[2Cu^{2+}, O^{2-}]^{2+}$ configuration.

Methane activation in $[Cu_2O]^{2+}$ is associated with the Cu^{2+}/Cu^+ redox couple. If the methyl group rebounds to another active site, $[Cu\text{-}OH\text{-}Cu]^{2+}$ and $[Cu\text{-}OCH_3\text{-}Cu]^{2+}$ are formed. These are of $[Cu^+, O^{2-}, Cu^{2+}]$ character. If the methyl is stabilized at the reacting active site, then [Cu-

$O(H)(CH_3)$-$Cu]^{2+}$ is formed. Stabilization of the methyl remotely at Brønsted acid site, BAS, leads to formation of $[Cu\text{-}OH\text{-}Cu]^{2+}$ or $[Cu\text{-}O(H)(H)\text{-}Cu]^{2+}$, with the latter involving proton exchange between the active site and the BAS. The overall processes leading to these 3 species still utilize the Cu^{2+}/Cu^{+} redox couple.

By contrast, there are many more possible intermediates for methane activation by $[Cu_3O_3]^{2+}$. We considered 9 possibilities. Species where the methyl group is stabilized at the μ-oxo atoms are driven by a combination of the Cu^{2+}/Cu^{+} and oxyl/O^{2-} redox couples. One electron is transferred to an oxyl site, reducing it to O^{2-} and the other electron is transferred to a Cu^{2+} center. Thus for these species, one mole of Cu^{+} is produced for each mole of methanol, assuming high selectivities. This is supported by examination of the canonical molecular orbitals and LOBA. Interestingly, when the methyl group is stabilized at a remote location (for example at BASs in exchange for a proton), Cu^{+} is still formed in the active site. Thus, the Cu^{2+}/Cu^{+} couple still participates for $[Cu_3O_3]^{2+}$ when separated methyl groups rebound to Brønsted acid sites. This is the same for species that are likely relevant at high methane pressures. Based on these findings, we hypothesized that methane activation on $[Cu_3O_3]^{2+}$ will be associated with spectroscopic features indicative of $Cu^{2+} \rightarrow Cu^{+}$ reduction. The signatures for $Cu^{2+} \rightarrow Cu^{+}$ reduction must also be similar for $[Cu_3O_3]^{2+}$ and $[Cu_2O]^{2+}$.

In a search for these spectroscopic signatures, we computed Cu 1s-edge XAS, before and after methane activation by $[Cu_2O]^{2+}$ and $[Cu_3O_3]^{2+}$. For the $[Cu_2O]^{2+}$ and $[Cu_3O_3]^{2+}$ intermediates containing 1 Cu^{+} center, there is a shift of 0.9-1.7 eV. For intermediates containing 2 Cu^{+} centers, we obtained shifts of 3.0-4.3 eV. These encompass shifts of 2.5-3.2 eV observed experimentally. Central to this work however is the fact that XAS shifts obtained for $[Cu_3O_3]^{2+}$ intermediates are similar to those of comparable $[Cu_2O]^{2+}$ species. Even with larger cluster models and a modest inclusion of structural dynamics, the $[Cu_3O_3]^{2+}$ intermediates still show significant XAS shifts. Our results favor a conclusion that activation of 1 or 2 methane molecules by $[Cu_3O_3]^{2+}$ will lead to formation of Cu^{+} sites. Lastly, involvement of $O^{-} + e^{-} \rightarrow O^{2-}$ in the $[Cu_3O_3]^{2+}$ systems implies a disconnect between overall reactivity and the number of electrons utilized in the Cu^{2+}/Cu^{+} redox couple.

■ ASSOCIATED CONTENT

Supporting Information.

The Supporting Information is available free of charge at https://

Optimized geometries of all systems considered in this work (PDF).

AUTHOR INFORMATION

Corresponding Authors

*S.O.O.: E-mail: sodoh@unr.edu

Notes

#These authors participated equally to this work. We declare no competing financial interest.

ACKNOWLEDGMENT

This material is based upon work supported by the National Science Foundation under Grant No. 1800387.

REFERENCES

(1) Dunn, S. Hydrogen futures: toward a sustainable energy system, *Int. J. Hydrogen Energy* **2002**, *27*,

(2) Olah, G. A. Beyond Oil and Gas: The Methanol Economy, *Angew. Chem. Int. Ed.* **2005**, *44*,

(3) Lunsford, J. H. Catalytic conversion of methane to more useful chemicals and fuels: a challenge for the 21st century, *Catal. Today* **2000**, *63*,

(4) Latimer, A. A.; Kakekhani, A.; Kulkarni, A. R.; Nørskov, J. K. Direct Methane to Methanol: The Selectivity–Conversion Limit and Design Strategies, *ACS Catal.* **2018**, *8*,

(5) de Klerk, A. Engineering evaluation of direct methane to methanol conversion, *Energy Sci. Eng.* **2015**, *3*,

(6) Dinh, K. T.; Sullivan, M. M.; Serna, P.; Meyer, R. J.; Dincă, M.; Román-Leshkov, Y. Viewpoint on the Partial Oxidation of Methane to Methanol Using Cu- and Fe-Exchanged Zeolites, *ACS Catal.* **2018**, *8*,

(7) Kim, Y.; Kim, T. Y.; Lee, H.; Yi, J. Distinct activation of Cu-MOR for direct oxidation of methane to methanol, *Chem. Commun.* **2017**, *53*,

(8) Koishybay, A.; Shantz, D. F. Water Is the Oxygen Source for Methanol Produced in Partial Oxidation of Methane in a Flow Reactor over Cu-SSZ-13, *J. Am. Chem. Soc.* **2020**, *142*,

(9) Narsimhan, K.; Iyoki, K.; Dinh, K.; Román-Leshkov, Y. Catalytic Oxidation of Methane into Methanol over Copper-Exchanged Zeolites with Oxygen at Low Temperature, *ACS Cent. Sci.* **2016**, *2*,

(10) Newton, M. A.; Knorpp, A. J.; Sushkevich, V. L.; Palagin, D.; van Bokhoven, J. A. Active sites and mechanisms in the direct conversion of methane to methanol using Cu in zeolitic hosts: a critical examination, *Chem. Soc. Rev.* **2020**, *49*,

(11) Park, M. B.; Park, E. D.; Ahn, W.-S. Recent Progress in Direct Conversion of Methane to Methanol Over Copper-Exchanged Zeolites, *Front. Chem.* **2019**, *7*,

(12) Snyder, B. E. R.; Bols, M. L.; Schoonheydt, R. A.; Sels, B. F.; Solomon, E. I. Iron and Copper Active Sites in Zeolites and Their Correlation to Metalloenzymes, *Chem. Rev.* **2018**, *118*,

(13) Tomkins, P.; Ranocchiari, M.; van Bokhoven, J. A. Direct Conversion of Methane to Methanol under Mild Conditions over Cu-Zeolites and beyond, *Acc. Chem. Res.* **2017**, *50*,

(14) Vogiatzis, K. D.; Li, G.; Hensen, E. J. M.; Gagliardi, L.; Pidko, E. A. Electronic Structure of the [Cu3(μ-O)3]2+ Cluster in Mordenite Zeolite and Its Effects on the Methane to Methanol Oxidation, *J. Phys. Chem. C* **2017**, *121*,

(15) Beznis, N. V.; Weckhuysen, B. M.; Bitter, J. H. Cu-ZSM-5 Zeolites for the Formation of Methanol from Methane and Oxygen: Probing the Active Sites and Spectator Species, *Catal. Lett.* **2010**, *138*,

(16) Brezicki, G.; Kammert, J. D.; Gunnoe, T. B.; Paolucci, C.; Davis, R. J. Insights into the Speciation of Cu in the Cu-H-Mordenite Catalyst for the Oxidation of Methane to Methanol, *ACS Catal.* **2019**, *9*,

(17) Kulkarni, A. R.; Zhao, Z.-J.; Siahrostami, S.; Nørskov, J. K.; Studt, F. Monocopper Active Site for Partial Methane Oxidation in Cu-Exchanged 8MR Zeolites, *ACS Catal.* **2016**, *6*,

(18) Ziegler, M. S.; Lakshmi, K. V.; Tilley, T. D. Dicopper Cu(I)Cu(I) and Cu(I)Cu(II) Complexes in Copper-Catalyzed Azide–Alkyne Cycloaddition, *J. Am. Chem. Soc.* **2017**, *139*,

(19) Dandu, N. K.; Adeyiga, O.; Panthi, D.; Bird, S. A.; Odoh, S. O. Performance of density functional theory for describing hetero-metallic active-site motifs for methane-to-methanol conversion in metal-exchanged zeolites, *J. Comput. Chem.* **2018**, *39*,

(20) Dandu, N. K.; Reed, J. A.; Odoh, S. O. Performance of Density Functional Theory for Predicting Methane-to-Methanol Conversion by a Tri-Copper Complex, *J. Phys. Chem. C* **2018**, *122*,

(21) Grundner, S.; Luo, W.; Sanchez-Sanchez, M.; Lercher, J. A. Synthesis of single-site copper catalysts for methane partial oxidation, *Chem. Commun.* **2016**, *52*,

(22) Grundner, S.; Markovits, M. A. C.; Li, G.; Tromp, M.; Pidko, E. A.; Hensen, E. J. M.; Jentys, A.; Sanchez-Sanchez, M.; Lercher, J. A. Single-site trinuclear copper oxygen clusters in mordenite for selective conversion of methane to methanol, *Nature Commun.* **2015**, *6*,

(23) Le, H. V.; Parishan, S.; Sagaltchik, A.; Göbel, C.; Schlesiger, C.; Malzer, W.; Trunschke, A.; Schomäcker, R.; Thomas, A. Solid-State Ion-Exchanged Cu/Mordenite Catalysts for the Direct Conversion of Methane to Methanol, *ACS Catal.* **2017**, *7*,

(24) Li, G.; Vassilev, P.; Sanchez-Sanchez, M.; Lercher, J. A.; Hensen, E. J. M.; Pidko, E. A. Stability and reactivity of copper oxo-clusters in ZSM-5 zeolite for selective methane oxidation to methanol, *J. Catal.* **2016**, *338*,

(25) Mahyuddin, M. H.; Tanaka, T.; Shiota, Y.; Staykov, A.; Yoshizawa, K. Methane Partial Oxidation over $[Cu_2(\mu\text{-}O)]^{2+}$ and $[Cu_3(\mu\text{-}O)_3]^{2+}$ Active Species in Large-Pore Zeolites, *ACS Catal.* **2018**, *8*,

(26) Newton, M. A.; Knorpp, A. J.; Pinar, A. B.; Sushkevich, V. L.; Palagin, D.; van Bokhoven, J. A. On the Mechanism Underlying the Direct Conversion of Methane to Methanol by Copper Hosted in Zeolites; Braiding Cu K-Edge XANES and Reactivity Studies, *J. Am. Chem. Soc.* **2018**, *140*,

(27) Becke, A. D. Perspective: Fifty years of density-functional theory in chemical physics, *J. Chem. Phys.* **2014**, *140*,

(28) Cohen, A. J.; Mori-Sánchez, P.; Yang, W. Challenges for Density Functional Theory, *Chem. Rev.* **2012**, *112*,

(29) Curtis, K.; Panthi, D.; Odoh, S. O. A Time-Dependent DFT Study of Copper (II) Oxo Active Sites for Methane-to-Methanol Conversion in Zeolites, *Inorg. Chem.* **2020**, *submitted*,

(30) Hirata, S.; Head-Gordon, M. Time-dependent density functional theory within the Tamm–Dancoff approximation, *Chem. Phys. Lett.* **1999**, *314*,

(31) Casanova-Páez, M.; Dardis, M. B.; Goerigk, L. ωB2PLYP and ωB2GPPLYP: The First Two Double-Hybrid Density Functionals with Long-Range Correction Optimized for Excitation Energies, *J. Chem. Theory Comput.* **2019**, *15*,

(32) Casanova-Páez, M.; Goerigk, L. Assessing the Tamm–Dancoff approximation, singlet–singlet, and singlet–triplet excitations with the latest long-range corrected double-hybrid density functionals, *J. Chem. Phys.* **2020**, *153*,

(33) Goerigk, L.; Casanova-Paéz, M. The Trip to the Density Functional Theory Zoo Continues: Making a Case for Time-Dependent Double Hybrids for Excited-State Problems, *Aust. J. Chem.* **2020**, CH20093.

(34) Adeyiga, O.; Suleiman, O.; Odoh, S. O. Copper Oxo Active Sites for Methane C-H Activation in Zeolites: Molecular Understanding of Impact of Methane Hydroxylation on UV-Vis Spectra, *Inorg. Chem.* **2020**, *submitted*,

(35) Vanelderen, P.; Snyder, B. E. R.; Tsai, M.-L.; Hadt, R. G.; Vancauwenbergh, J.; Coussens, O.; Schoonheydt, R. A.; Sels, B. F.; Solomon, E. I. Spectroscopic Definition of the Copper Active Sites in Mordenite: Selective Methane Oxidation, *J. Am. Chem. Soc.* **2015**, *137*,

(36) Ikuno, T.; Grundner, S.; Jentys, A.; Li, G.; Pidko, E.; Fulton, J.; Sanchez-Sanchez, M.; Lercher, J. A. Formation of Active Cu-oxo Clusters for Methane Oxidation in Cu-Exchanged Mordenite, *J. Phys. Chem. C* **2019**, *123*,

(37) Kokotailo, G. T.; Lawton, S. L.; Olson, D. H.; Meier, W. M. Structure of synthetic zeolite ZSM-5, *Nature* **1978**, *272*,

(38) Groothaert, M. H.; Smeets, P. J.; Sels, B. F.; Jacobs, P. A.; Schoonheydt, R. A. Selective Oxidation of Methane by the Bis(μ-oxo)dicopper Core Stabilized on ZSM-5 and Mordenite Zeolites, *J. Am. Chem. Soc.* **2005**, *127*,

(39) Groothaert, M. H.; van Bokhoven, J. A.; Battiston, A. A.; Weckhuysen, B. M.; Schoonheydt, R. A. Bis(μ-oxo)dicopper in Cu-ZSM-5 and Its Role in the Decomposition of NO: A Combined in Situ XAFS, UV−Vis−Near-IR, and Kinetic Study, *J. Am. Chem. Soc.* **2003**, *125*,

(40) Woertink, J. S.; Smeets, P. J.; Groothaert, M. H.; Vance, M. A.; Sels, B. F.; Schoonheydt, R. A.; Solomon, E. I. A [Cu2O]2+ core in Cu-ZSM-5, the active site in the oxidation of methane to methanol, *Proc Natl Acad Sci U S A* **2009**, *106*,

(41) Mahyuddin, M. H.; Shiota, Y.; Yoshizawa, K. Methane selective oxidation to methanol by metal-exchanged zeolites: a review of active sites and their reactivity, *Catal. Sci. Technol.* **2019**, *9*,

(42) Zheng, J.; Lee, I.; Khramenkova, E.; Wang, M.; Peng, B.; Gutiérrez, O. Y.; Fulton, J. L.; Camaioni, D. M.; Khare, R.; Jentys, A.; Haller, G. L.; Pidko, E. A.; Sanchez-Sanchez, M.; Lercher, J. A. Importance of Methane Chemical Potential for Its Conversion to Methanol on Cu-Exchanged Mordenite, *Chem-Eur. J.* **2020**, *26*,

(43) Grimme, S.; Antony, J.; Ehrlich, S.; Krieg, H. A consistent and accurate ab initio parametrization of density functional dispersion correction (DFT-D) for the 94 elements H-Pu, *J. Chem. Phys.* **2010**, *132*,

(44) Grimme, S.; Ehrlich, S.; Goerigk, L. Effect of the damping function in dispersion corrected density functional theory, *J. Comput. Chem.* **2011**, *32*,

(45) Becke, A. D.; Johnson, E. R. A density-functional model of the dispersion interaction, *J. Chem. Phys.* **2005**, *123*,

(46) Becke, A. D.; Johnson, E. R. Exchange-hole dipole moment and the dispersion interaction: High-order dispersion coefficients, *J. Chem. Phys.* **2006**, *124*,

(47) Laun, J.; Vilela Oliveira, D.; Bredow, T. Consistent gaussian basis sets of double- and triple-zeta valence with polarization quality of the fifth period for solid-state calculations, *J. Comput. Chem.* **2018**, *39*,

(48) Becke, A. D. Density-functional thermochemistry. III. The role of exact exchange, *J. Chem. Phys.* **1993**, *98*,

(49) Lee, C.; Yang, W.; Parr, R. G. Development of the Colle-Salvetti correlation-energy formula into a functional of the electron density, *Physical Review B* **1988**, *37*,

(50) Cramer, C. J.; Truhlar, D. G. Density functional theory for transition metals and transition metal chemistry, *Phys. Chem. Chem. Phys.* **2009**, *11*,

(51) Thom, A. J. W.; Sundstrom, E. J.; Head-Gordon, M. LOBA: a localized orbital bonding analysis to calculate oxidation states, with application to a model water oxidation catalyst, *Phys. Chem. Chem. Phys.* **2009**, *11*,

(52) Lenthe, E. v.; Snijders, J. G.; Baerends, E. J. The zero-order regular approximation for relativistic effects: The effect of spin–orbit coupling in closed shell molecules, *J. Chem. Phys.* **1996**, *105*,

(53) Pantazis, D. A.; Neese, F. All-Electron Scalar Relativistic Basis Sets for the Actinides, *J. Chem. Theory Comput.* **2011**, *7*,

(54) Weigend, F.; Ahlrichs, R. Balanced basis sets of split valence, triple zeta valence and quadruple zeta valence quality for H to Rn: Design and assessment of accuracy, *Phys. Chem. Chem. Phys.* **2005**, *7*,

(55) Adamo, C.; Barone, V. Toward reliable adiabatic connection models free from adjustable parameters, *Chem. Phys. Lett.* **1997**, *274*,

(56) Becke, A. D. Density-functional exchange-energy approximation with correct asymptotic behavior, *Physical Review A* **1988**, *38*,

(57) Tomson, N. C.; Williams, K. D.; Dai, X.; Sproules, S.; DeBeer, S.; Warren, T. H.; Wieghardt, K. Re-evaluating the Cu K pre-edge XAS transition in complexes with covalent metal–ligand interactions, *Chem. Sci.* **2015**, *6*,

(58) Neese, F. The ORCA program system, *WIREs Comput. Mol. Sci.* **2012**, *2*,

(59) Neese, F. Software update: the ORCA program system, version 4.0, *WIREs Comput. Mol. Sci.* **2018**, *8*,

(60) Lu, T.; Chen, F. Multiwfn: A multifunctional wavefunction analyzer, *J. Comput. Chem.* **2012**, *33*,

(61) Alayon, E. M. C.; Nachtegaal, M.; Bodi, A.; van Bokhoven, J. A. Reaction Conditions of Methane-to-Methanol Conversion Affect the Structure of Active Copper Sites, *ACS Catal.* **2014**, *4*,

(62) Borfecchia, E.; Pappas, D. K.; Dyballa, M.; Lomachenko, K. A.; Negri, C.; Signorile, M.; Berlier, G. Evolution of active sites during selective oxidation of methane to methanol over Cu-CHA and Cu-MOR zeolites as monitored by operando XAS, *Catal. Today* **2019**, *333*,

(63) Pappas, D. K.; Kvande, K.; Kalyva, M.; Dyballa, M.; Lomachenko, K. A.; Arstad, B.; Borfecchia, E.; Bordiga, S.; Olsbye, U.; Beato, P.; Svelle, S. Influence of Cu-speciation in mordenite on direct methane to methanol conversion: Multi-Technique characterization and comparison with NH3 selective catalytic reduction of NOx, *Catal. Today* **2020**,

(64) Li, H.; Paolucci, C.; Khurana, I.; Wilcox, Laura N.; Göltl, F.; Albarracin-Caballero, J. D.; Shih, A. J.; Ribeiro, F. H.; Gounder, R.; Schneider, W. F. Consequences of exchange-site heterogeneity and dynamics on the UV-visible spectrum of Cu-exchanged SSZ-13, *Chem. Sci.* **2019**, *10*, 2373.

For Table of Contents Only

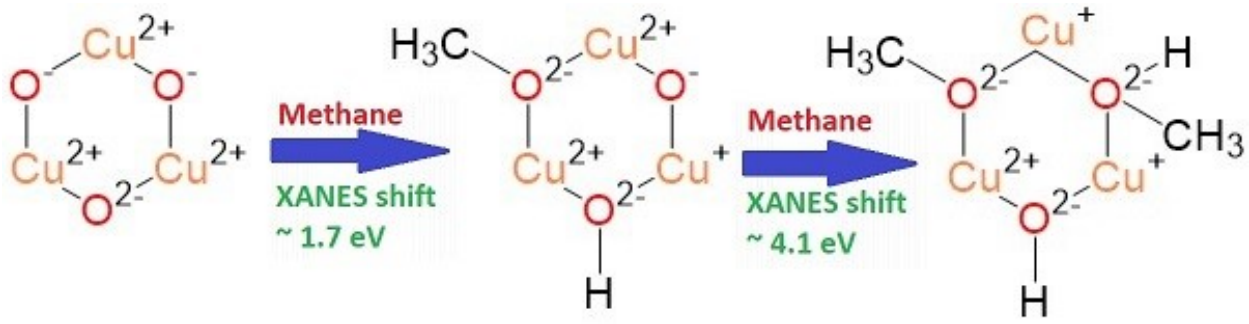

Synopsis: Details of methane activation by $[Cu_2O]^{2+}$ and $[Cu_3O_3]^{2+}$ active sites are investigated with DFT calculations, localized bonding orbital analysis (LOBA) and calculated Cu 1s-edge XANES spectra. For $[Cu_2O]^{2+}$, methane activation is clearly linked to the Cu^{2+}/Cu^{+} redox couple. Although, there are many possible intra-zeolite intermediates, methane activation by $[Cu_3O_3]^{2+}$ involves the Cu^{2+}/Cu^{+} and oxyl/O^{2-} redox couples. This finding is supported by the calculated XANES spectra.